Microporous and Mesoporous Materials 240 (2017) 123–129

Contents lists available at ScienceDirect

Microporous and Mesoporous Materials

journal homepage: www.elsevier.com/locate/micromeso

Dry-gel synthesis of mesoporous MFI zeolite nanosponges using a structure-directing surfactant

Seung Won Han [a, b], Jaeheon Kim [b], Ryong Ryoo [b, a, *]

[a] Department of Chemistry, Korea Advanced Institute of Science and Technology(KAIST), Daejeon 34141, Republic of Korea
[b] Center for Nanomaterials and Chemical Reactions, Institute for Basic Science(IBS), Daejeon 34141, Republic of Korea

ARTICLE INFO

Article history:
Received 5 October 2016
Received in revised form
9 November 2016
Accepted 15 November 2016
Available online 16 November 2016

Keywords:
Dry-gel conversion
Zeolite nanosheets
Mesoporous MFI zeolites
Hierarchical zeolites
Structure-directing surfactants

ABSTRACT

The synthesis of mesoporous MFI zeolite nanosponges was investigated in a dry-gel conversion process using $C_{18}H_{37}-N^+(CH_3)_2-C_6H_{12}-N^+(CH_3)_2-C_4H_9$ as a micropore-mesopore hierarchical structure-directing surfactant. The initial synthesis mixture was converted at 333 K to a mesoporous material exhibiting a structure similar to that of MCM-41. The mesoporous material was filtered, dried at 373 K, and subsequently heated at 423 K in an autoclave with controlled humidity. In this process, precise control of the relative chamber humidity and the pH of the precursor gel was necessary to achieve full crystallization of the zeolite. The final product was composed of three-dimensional networks of 2.5-nm thick MFI nanolayers and exhibited a high surface area and narrow distribution of mesopore diameters centered at 4 nm. The zeolite crystallization behavior at 423 K was investigated after various heating times with X-ray diffraction, gas adsorption, and electron microscopy. The results indicated that under controlled humidity, crystallization took place through a pseudomorphic transformation, where the initial gel morphology was maintained throughout. The overall quality of the dry-gel product was similar to that of a conventional hydrothermal product. The Si/Al ratios of the zeolite could be controlled over the range of 50 ~ ∞. Furthermore, in a 100-g synthesis batch, the dry-gel method had the advantage of compact autoclave size for large-scale synthesis.

© 2016 Elsevier Inc. All rights reserved.

1. Introduction

Zeolites are crystalline aluminosilicates that contain pores and cavities of molecular dimensions, which provide size and shape selectivity of guest molecules entering the zeolite pores [1,2]. Zeolites are the most important heterogeneous acid catalyst used in industry due to their strong acidity, uniform and small size pores, and high internal surface area [3]. Zeolites are widely used in selective separation processes [4,5] as well as in catalysis for oil refining and petrochemistry [3,6]. However, one drawback of zeolites is mass transfer and diffusion limitations for bulky molecules due to their small micropores [7–9]. To resolve such problems, many researchers have synthesized hierarchical zeolites containing a secondary pore system and nanocrystalline zeolites through top-down [10–15] or bottom-up [16–21] approaches using hard templates [18,19], soft templates [20,21], and post-synthetic treatments [12–14]. The diffusion challenges can be alleviated with the introduction of secondary porosity which allows facile diffusion of bulky reactants before micropore blocking by coking [8].

In 2009, the synthesis of extremely thin MFI zeolite nanosheets by the use of multi-ammonium surfactant molecules as a structure-directing agent (SDA) was reported [22]. These ultrathin zeolite nanosheets exhibited outstanding performance compared to bulk zeolite in various catalytic applications. Surfactant-directed synthesis has gained much attention since then as the thickness of the zeolite nanolayers and the porosity could be systematically controlled by modifying the number of ammonium groups and chain length of the surfactant, respectively [20,23,24]. However, the long hydrothermal synthesis time, broad distribution of mesopore sizes, and the collapse of the structure upon calcination were major impediments for practical applications of the zeolite nanosheets [25]. Notably, in 2014, a mesoporous MFI zeolite with a nanosponge-like morphology was hydrothermally synthesized by bulk crystal seeding using a diquaternary ammonium surfactant [26]. In this work, the addition of a small amount of bulk MFI zeolite seed crystals in the synthetic gel allowed the formation of MFI

* Corresponding author. Department of Chemistry, KAIST, Daejeon 34141, Republic of Korea.
E-mail address: rryoo@kaist.ac.kr (R. Ryoo).

http://dx.doi.org/10.1016/j.micromeso.2016.11.016
1387-1811/© 2016 Elsevier Inc. All rights reserved.

zeolite nanosponges that were composed of disordered networks of 2.5-nm-thick zeolite nanolayers, which were self-arranged to create uniformly-sized mesopores. The nanosponge morphology was rigidly self-retained by branched nanosheets, and accordingly, the mesoporosity was not negatively affected by adsorption of adsorbents and metal catalyst loading for catalytic applications [27–29]. The mechanical stability of the mesopore system up to 625 MPa compression was also confirmed [26]. These MFI zeolite nanosponges were applied in various reactions as an acid catalyst and a support material [27–29].

The conventional hydrothermal synthesis method used for the synthesis of MFI zeolite nanosponges poses some safety and environmental concerns associated with large reactor volume, high autogenous pressure of the reactor generated at elevated temperatures and the generation of massive waste material during synthesis [30]. Such problems make the large scale production of zeolite nanosponges less practical. As an alternative solution, dry-gel conversion (DGC) method can be implemented. In this method, a hydrogel is dried, and the dried precursor gel is directly transformed into crystalline zeolite with the assistance of steam [31]. DGC is a more environment-friendly and economic method for zeolite synthesis since it allows significant reductions of reactor volume and reaction pressure because a small amount of solvent is used for the synthesis [30–32]. In addition, DGC has the advantages of a higher zeolite yield, rapid crystallization, and conservation of the synthesis gel composition [30–32]. The application of DGC in zeolite synthesis was first introduced by Xu *et al.* in 1990 [33]. They reported the direct conversion of dry aluminosilicate gel into MFI zeolite in the presence of steam and amine vapor. More recently, solvent-free synthesis method which completely avoids the addition of solvent was introduced to synthesize various types of zeolites with high synthesis efficiency [34,35]. Although the DGC method has been employed in the synthesis of various kinds of zeolites [31–33,36–43], it has never been carried out to synthesize mesoporous zeolites using multi-ammonium structure-directing surfactants.

In the present work, the DGC synthesis of MFI zeolite nanosponges using a dual-templating diquaternary ammonium surfactant was successfully demonstrated. After a careful adjustment of the synthesis condition parameters, such as the chamber humidity and the pH of the zeolite precursor, we were able to precisely control the synthesis conditions to obtain MFI zeolite nanosponges with an overall quality comparable to that of hydrothermally synthesized zeolite nanosponges. Furthermore, we were able to synthesize 100 g of MFI zeolite nanosponges in a single stainless steel autoclave with a volume of 1.5 L. The resultant zeolite product possessed a high surface area and uniform distribution of mesopore diameters. The crystallization behavior of the dry-gel synthesized MFI zeolite nanosponges was investigated by various analytic techniques, including X-ray diffraction (XRD), scanning electron microscopy (SEM), transmission electron microscopy (TEM), and gas sorption analysis. The synthesis of mesoporous MFI zeolite nanosponges with various Si/Al ratios was performed using the advantages of the DGC technique.

2. Experimental

2.1. Synthesis of MFI zeolite nanosponges by dry-gel conversion

MFI zeolite nanosponges were synthesized using $[C_{18}H_{37}–N^+(CH_3)_2–C_6H_{12}–N^+(CH_3)_2–C_4H_9]Br_2$ (abbreviated hereafter as $C_{18\text{-}6\text{-}4}$) as SDA, which was prepared following the procedure described in the literature [26]. In a typical synthesis of MFI nanosponges with Si/Al = 50, a precursor gel was prepared as follows. First, 8.29 g of sodium silicate solution (water glass, 29 wt% SiO_2, Si/Na = 1.75, Shinheung Silicate) was added slowly dropwise to an aqueous solution containing 1.93 g of $C_{18\text{-}6\text{-}4}$ and 0.27 g of $Al_2(SO_4)_3 \cdot 18H_2O$ (Sigma Aldrich). The gel mixture was vigorously shaken by hand and heated at 333 K for 3 h under stirring. To adjust the pH of the mixture to 12, 1.00 g of 47% sulfuric acid (Wako Chemicals) was added dropwise. After the mixture was shaken by hand and left under stirring at 333 K for 6 h, 0.12 g of commercial MFI zeolite (5 wt% of total silica, Zeolyst, Si/Al = 40) was added as seeds. The mixture had the following molar composition: 100 SiO_2/1 Al_2O_3/7.5 $C_{18\text{-}6\text{-}4}$/28.6 Na_2O/15 H_2SO_4/6000 H_2O. This mixture was heated for 1 d at 333 K under stirring, and the resultant precipitate was filtered and dried in a 373 K oven for 2 h. The dried precipitate (or dry gel) was put in a Pyrex beaker. The beaker was then placed in a Teflon-lined autoclave (150 cm^3), which contained a 6.9-M aqueous solution of ammonium nitrate in the bottom. The chamber humidity during the synthesis was controlled to 80% by the salt concentration, as described in the literature [43]. The autoclave containing the dry gel was heated at 423 K for 3.5 d under a static condition. The obtained product was washed with distilled water and calcined at 823 K for 4 h (ramping rate of 2.3 K min^{-1}) in air to remove the SDA.

2.2. Product characterization

Powder XRD patterns were recorded on a Rigaku Multiflex X-ray diffractometer using nickel-filtered Cu Kα radiation (λ = 0.1541 nm, 30 kV, 40 mA). The XRD patterns were obtained under ambient conditions with a 0.05° step and an accumulation time of 0.3 s. SEM images were taken using a field emission scanning electron microscope (FEI, Verios 460) at an accelerating voltage of 5 kV and a decelerating voltage of 4 kV, to have a landing voltage of 1 kV. The powder sample for SEM imaging was dispersed on a carbon tape and kept under vacuum for 1 h before the imaging. TEM images were obtained using Titan G^2 ETEM (FEI) at an accelerating voltage of 300 kV. The powder sample for TEM imaging was prepared by dropping a small amount of acetone containing a suspended powder sample on a holey carbon film-coated 300 mesh copper grid. The specific surface area, pore size distribution and pore volume were determined from N_2 adsorption-desorption isotherms measured at 77 K using a Micromeritics TriStar II instrument. Samples were outgassed at 573 K for 3 h prior to the measurement. The specific surface area was calculated using the Brunauer-Emmett-Teller (BET) equation from the adsorption data in the region of $0.06 < P/P_0 < 0.2$. The micropore volume was calculated by the *t*-plot methods. The pore size distribution was determined using the Barret-Joyner-Halenda (BJH) method. The adsorption branch of the isotherm was used to calculate mesopore size distribution and total pore volume. The Si/Al ratios were determined by inductively coupled plasma optical emission spectrometry (ICP-OES) using iCAP 6300 Duo (Thermo Scientific).

3. Results and discussion

3.1. Synthesis of MFI zeolite nanosponges with Si/Al = 50 by DGC

In zeolite synthesis by DGC, the chamber humidity during crystallization and the pH of the initial synthetic mixture are considered important factors that greatly affect zeolite formation [32,40,43,44]. Since DGC proceeds in the presence of a small amount of water that does not come into direct contact with the dry gel, the chamber humidity can be varied by changing the amount of water to control the mass transfer of silicate species during crystallization [43]. The basicity (or pH) of the initial synthetic mixture is also a critical factor as it is in the case for hydrothermal synthesis. The pH value can significantly influence the final

zeolite product, phase purity, and zeolite crystallization behavior, such as the rate of nucleation and crystallization [2]. Such factors were considered in various zeolite syntheses by DGC, such as SDA-free synthesis of ultrafine zeolites [42], synthesis of hierarchical zeolites using mesoporous carbon templates [43], and synthesis of SAPO-11 [44].

In this regard, we optimized the synthesis conditions of MFI zeolite nanosponges by modifying the relative chamber humidity and the pH of the initial starting mixture through a trial-and-error process. The optimized gel composition was 100 SiO_2/1 Al_2O_3/7.5 $C_{18\text{-}6\text{-}4}$/28.6 Na_2O/15 H_2SO_4/6000 H_2O. Highly mesoporous MFI zeolite nanosponges were synthesized using this composition and a relative chamber humidity above 80% in 3.5 d of reaction time. When the humidity was set to 80%, the morphology of the initial dry gel was retained in the final zeolite product (Supplementary Fig. 1). At this humidity condition, the amount of water present was high enough to transform the precursor into zeolite crystals but low enough for transformation to occur in a pseudomorphic manner. At 100% humidity, silicate species seemed to migrate easily through the liquid phase formed by condensation in the initial gel as in the zeolite synthesis inside mesoporous carbon templates [43]. The transformation of the precursor into crystalline zeolite under this circumstance was not pseudomorphic, and the morphology of the final product resembled that of hydrothermally synthesized MFI zeolite nanosponges (Supplementary Fig. 1). The sizes of the nanosponge particles were larger for products obtained at 100% humidity than for products obtained at 80% humidity, indicating that zeolite formation could occur fully by dissolution-crystallization processes as in hydrothermal conditions. On the other hand, when the humidity was lowered to 50% and 60%, the rate of zeolite formation was decelerated (Supplementary Fig. 2). This can be attributed to the suppressed migration of zeolite precursors at low humidity. Therefore, all the syntheses were performed at 80% humidity in the remainder of this work.

In DGC synthesis at 80% humidity, fully crystalline zeolite nanosponges were obtained only within a certain pH range. The optimized pH for the synthesis was 12, and this value was precisely controlled by the addition of sulfuric acid to reduce the alkalinity as mentioned in the Experimental section. The synthesis condition parameters and the products obtained with various amounts of sulfuric acid presented in Table 1. This table shows that samples 1, 2, and 4 contained a combination of MFI zeolite nanosponges and amorphous phases. Smaller amounts of zeolite product were detected at higher pH conditions (samples 1 and 2), which was probably due to the difficulty of seed generation under highly basic conditions. In the case of sample 4, which was prepared with a relatively low pH gel condition, the majority of the sample was crystalline zeolite nanosponge with a minor presence of amorphous phase. This result suggests that an appropriate amount of sulfuric acid is necessary to depolymerize the silica gel and initiate the nucleation process simultaneously.

After the fine tuning of the synthesis condition parameters and gel composition, we were able to successfully obtain MFI zeolite nanosponges with Si/Al ratio of 50 by DGC. The structure of the final zeolite product was investigated by a complementary combination of XRD, N_2 adsorption, SEM, and TEM. Fig. 1A and B shows representative SEM and TEM images of the DGC synthesized product. The zeolite product exhibited a nanosponge-like morphology constructed by disordered stacking of 2.5-nm-thick crystalline MFI nanolayers. These nanolayers were self-supported mostly in the form of pillared layers forming a three-dimensional network. The zeolite sample was highly crystalline after 3.5 d of heating without any significant presence of amorphous particles, bulk MFI zeolite particles, or other impurities as observed in the electron microscope images. The structure of the zeolite product was assessed by low- and high-angle powder XRD patterns (Fig. 1C). The high-angle XRD pattern contained peaks showing the characteristic Bragg reflections of an MFI-type zeolite. The peaks at 7.9, 8.9, 23.1, and 23.9° correspond to (101), (200), (501), and (303) reflections, respectively. The low-angle pattern, which contains information about the mesoporous structure of zeolite, showed a peak at 1.5°. This peak can be attributed to the uniform spacing between the adjacent nanolayers as shown in the TEM image (Fig. 1B).

The porous texture of the obtained zeolite product was examined by N_2 adsorption analysis. Fig. 1D and E shows the N_2 adsorption-desorption isotherm and its corresponding pore size distribution. The isotherm exhibited a type IV isotherm with a hysteresis loop in the range of $0.4 < P/P_0 < 0.9$, which can be explained by the capillary condensation occurring inside the mesopores formed by the spacing between the nanolayers. A sharp increase in the region of $P/P_0 < 0.01$ can be attributed to the filling of micropores within the zeolite framework. This result, in correspondence with the previous XRD analysis, confirmed that the product was a highly crystalline zeolite. The surface area was calculated using the BET model to be 560 $m^2\ g^{-1}$. The total pore volume was 0.57 $cm^3\ g^{-1}$, which could be further categorized into the micropore volume of 0.10 $cm^3\ g^{-1}$ and the mesopore volume of 0.47 $cm^3\ g^{-1}$. The pore size analysis was performed based on the BJH method and the pore size distribution plot shows a narrow peak centered at 3.8 nm, which resembles the size of surfactant micelles formed during synthesis. Such presence of mesopores in the zeolite product was again consistent with the electron microscopy results noted above.

Furthermore, the accurate control of synthesis condition parameters allowed scale-up synthesis of MFI zeolite nanosponges. A stainless steel autoclave with a volume of 1.5 L equipped with a specially designed Teflon cup, which allowed the separation of the zeolite precursor and the ammonium nitrate solution, was used for the large scale synthesis (Supplementary Fig. 3). The scale-up synthesis yielded 100 g of zeolite nanosponge from a single reactor. The quality of the zeolite product was similar throughout the sample, proving a good diffusion of the water

Table 1
Synthesis conditions and product characterization of MFI zeolite nanosponge products obtained at 80% humidity.

No.	Gel composition					Product characterization			
	SiO_2	Al_2O_3	SDA	H_2SO_4	H_2O	Phase[a]	S_{BET}[b] ($m^2\ g^{-1}$)	V_t[c] (cc g^{-1})	D_{BJH}[d] (nm)
1	100	1	7.5	13	6000	MFI, amorphous	659	0.58	3.3
2	100	1	7.5	14	6000	MFI, amorphous	599	0.56	3.3
3	100	1	7.5	15	6000	MFI	568	0.72	3.8
4	100	1	7.5	17	6000	MFI, amorphous	493	0.55	3.6

[a] The phase of zeolite product was determined by examining SEM and TEM images.
[b] Surface area calculated using the BET method from the adsorption branch in the region of $0.06 < P/P_0 < 0.2$.
[c] The total pore volume at a relative pressure of 0.97.
[d] The mode diameter of mesopores calculated from adsorption branch by the BJH method.

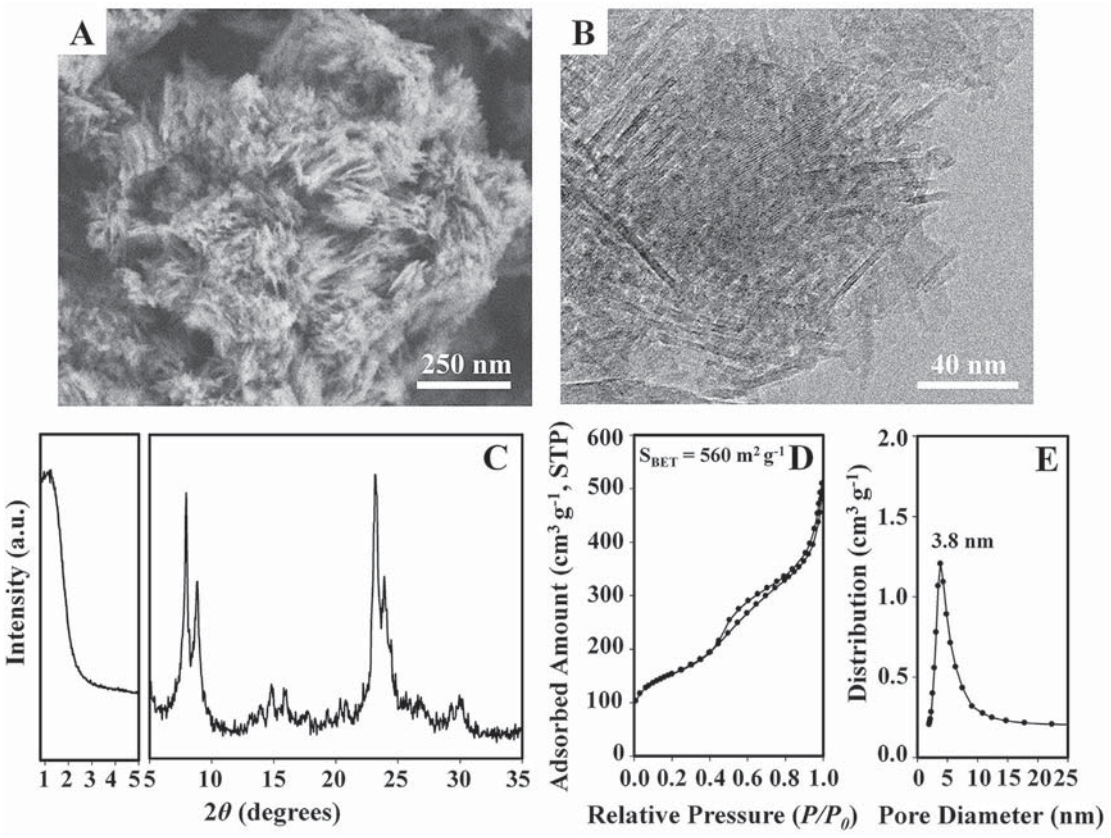

Fig. 1. Representative SEM image (A), TEM image (B), XRD pattern (C), N_2 adsorption-desorption isotherm (D), and BJH pore size distribution (E) of MFI zeolite nanosponges with Si/Al = 50 synthesized under synthesis condition 3 given in Table 1.

vapor into the precursor gel. The final zeolite product was also composed of thin MFI zeolite nanolayers stacked in a disordered manner, and they exhibited a large BET surface area with narrow mesopore size distribution. This suggests that the DGC route of synthesizing MFI zeolite nanosponges is a promising method for scale-up synthesis.

3.2. The zeolite formation behavior of MFI zeolite nanosponges during DGC

The zeolite formation mechanism of dry-gel synthesized MFI zeolite nanosponges was studied through an investigation of products collected at various periods of heating at 423 K. The optimized gel composition mentioned in the Experimental section was used for this investigation. Fig. 2 shows the powder XRD patterns of the calcined product collected during the period of 0–3.5 d of crystallization. The MFI characteristic Bragg reflection peaks started to appear for the zeolite intermediate collected at 1 d, and their intensities continued to increase with crystallization time, reaching a maximum at 3.5 d of crystallization. The low-angle XRD patterns provided valuable information about the transformation of the mesoporous structure throughout the zeolite synthesis. The initial gel had an ordered hexagonal mesostructure similar to that of MCM-41-type amorphous silica ($2\theta_{100} = 2.0°$, $2\theta_{110} = 3.5°$). As crystallization proceeded, a peak corresponding to a larger d-spacing ($2\theta_{100} = 1.5°$) was observed. This new peak in the low-angle region can be assigned to the spacing between the crystalline MFI zeolite walls stacked in a disordered manner, forming a nanosponge-like mesoporous structure. The TEM images shown in Supplementary Fig. 4 are consistent with the structural changes

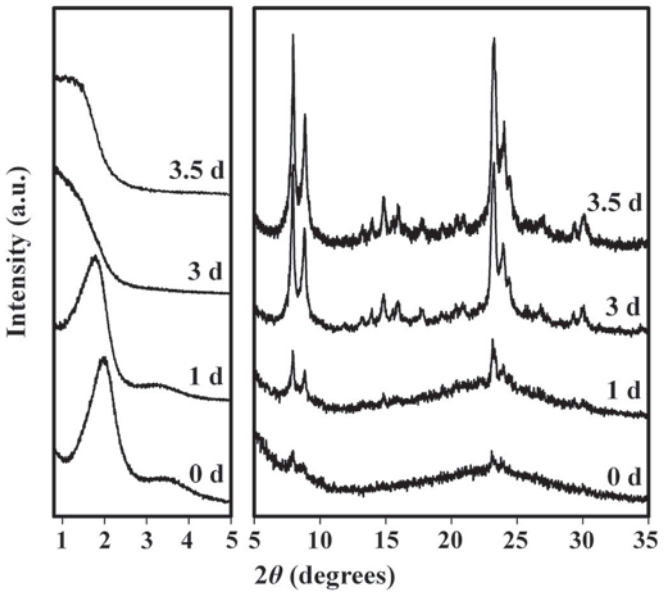

Fig. 2. XRD patterns of the dry-gel synthesized zeolite products in the calcined form periodically collected after various crystallization times, under synthesis condition 3 given in Table 1.

determined by the XRD patterns above. The initial phase consisting of an ordered hexagonal mesophase with amorphous walls was dominant up to 3 d and was completely converted to crystalline zeolite phase after 3.5 d.

The structural transformations were further analyzed by SEM (Fig. 3), which allowed visualization of the zeolite products. In the process of crystallization, several phase transitions were observed. After 1 d of heating under the assistance of steam, an amorphous phase was dominant. As the synthesis proceeded, an intermediate lamellar phase with bent sheet-like morphology emerged and was later converted to a crystalline phase composed of thin MFI zeolite walls. The appearance of crystalline zeolite phase was first noticed on the outer surface of the crystal after 2 d of heating, which was as expected since water vapor had contact with the precursor gel on the outer surface first. As mentioned in the previous section, with a relative humidity of 80%, the morphology of the final product showed preservation of the initial precursor gel morphology. In this case, the crystallization occurred with a limited amount of water. Since transformation occured selectively where the water vapor was condensed in the precursor gel, the dissolution-recrystallization process was significantly limited and the initial gel morphology was able to be retained.

The mesopore texture of the zeolite products was characterized by N_2 adsorption-desorption isotherms collected at 77 K (Supplementary Fig. 5). The mesopore size distribution plot of the initial precursor determined by the BJH method showed two peaks centered at 3.3 and 13 nm. The narrow peak centered at 3.3 nm was shifted to 3.8 nm as the crystalline zeolite appeared and the broad peak at 13 nm disappeared, proving that a transformation of the mesoporous structure has occurred. Moreover, the microporous structure was examined by Ar adsorption-desorption isotherms collected at 87 K. The micropore volume of the product collected after various crystallization times was calculated using non-local density functional theory (NLDFT) to investigate the rate of zeolite crystallization. A typical S-shaped curve was achieved, implying that there was a short induction period followed by an acceleration of the crystallization (Supplementary Fig. 6). The micropore volume of the final product was 0.11 $cm^3\ g^{-1}$, which was similar to that of the hydrothermally prepared MFI zeolite nanosponges (0.13 $cm^3\ g^{-1}$) previously reported in the literature [26]. The crystallization behavior of the dry-gel synthesized MFI zeolite nanosponges was similar to that of a hydrothermal-synthesized product, except that in the case of the dry-gel synthesized zeolite nanosponges, pseudomorphic transformation was observed as the amount of water in contact with the zeolite crystal was limited to the amount of water that could be condensed inside the gel pores by capillary condensation. Since a combination of solution-mediated transformation mechanism and solid-state mechanism is employed for DGC, pseudomorphic transformation of the zeolite precursor to zeolite crystals was achieved.

3.3. Synthesis of MFI zeolite nanosponges with various Si/Al ratios

The synthesis of MFI zeolite nanosponges with a Si/Al ratio in the range of 50 to infinity was easily achieved using the DGC technique. In general, the rate of crystallization is longer for MFI zeolites with higher alumina content. This can be explained by the necessity of incorporating aluminum in the zeolite framework at the same time with exchange cations [25]. In the case of MFI zeolite nanosponges, crystallization was unsuccessful as the alumina content was increased. For the zeolite product with Si/Al = 30, crystallization was incomplete even after 5 d of steaming at 423 K. A lot of amorphous phase was still present even at 5 d (Supplementary Fig. 7A). After 7 d of steaming, a mixture of amorphous phase, MFI zeolite nanosponges, and bulk MFI zeolite was observed by SEM (Supplementary Fig. 7B). This phenomenon could be attributed to the partial decomposition of the SDA due to Hofmann elimination. For the synthesis of zeolite nanosponges

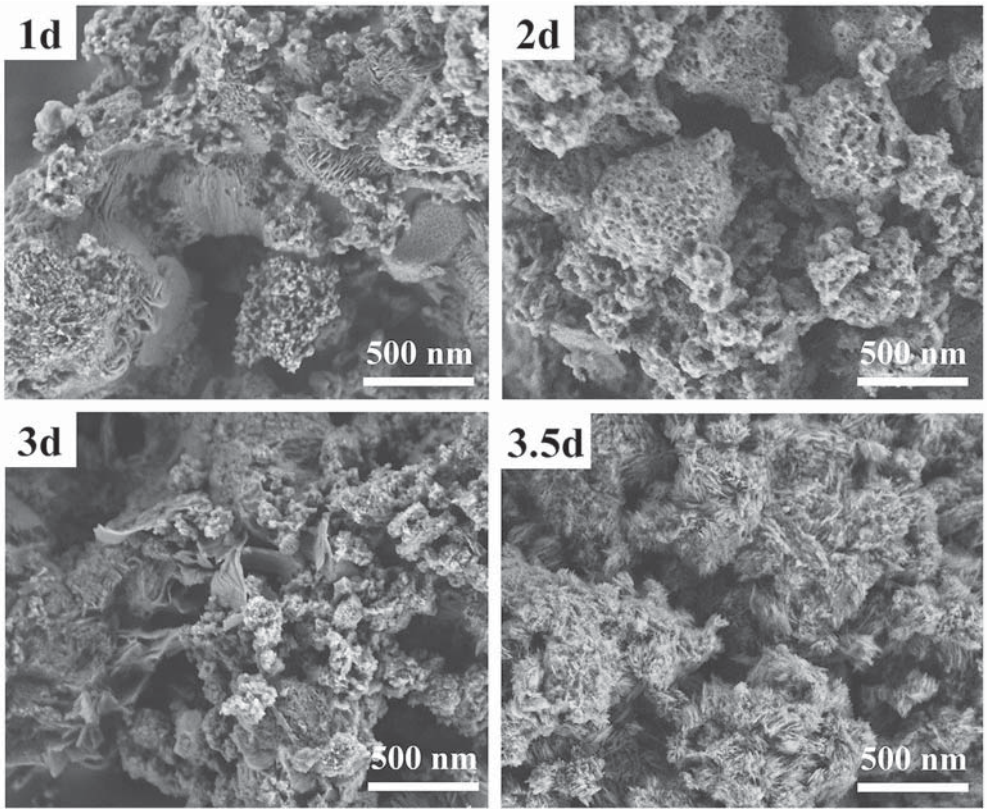

Fig. 3. SEM images of the dry-gel synthesized zeolite products in the calcined form periodically collected after various crystallization times, under synthesis condition 3 given in Table 1.

with a lower Si/Al ratio, the stability of the SDA under a highly basic condition had to be considered since the SDA was decomposed as the crystal growth rate was significantly decelerated.

On the other hand, MFI zeolite nanosponges in the form of pure silica were easily synthesized by DGC technique. Crystallization was successfully achieved after 3 d of steaming at 423 K. The structure of the purely siliceous MFI zeolite sample was characterized by XRD, SEM, TEM, and N_2 adsorption-desorption (Fig. 4). The structural analysis showed that the zeolite sample had a disordered mesoporous structure with a highly crystalline MFI framework and uniform mesopore diameters, similar to the zeolite nanosponges with Si/Al = 50. The nitrogen adsorption isotherm exhibited type IV isotherm with a capillary condensation step in the region of $0.4 < P/P_0$, which confirms the presence of mesopores. The pore size distribution of the pure silica form nanosponge zeolite exhibited a narrower distribution of mesopores than the nanosponge zeolite product with Si/Al = 50. The purely siliceous zeolite product was obtained within 3 d of crystallization time. As no aluminum incorporation into the framework was needed in this case, the crystallization time could be shortened. The dry-gel synthesis of zeolites allows easy control of the Si/Al ratio in the range of high Si content. Accordingly, the appropriate range of the Si/Al ratio was restricted to Si/Al $\geq$ 50.

In addition, the Si/Al ratio of the zeolite nanosponges was very close to the Si/Al ratio of the initial gel composition. In the case of the initial gel with Si/Al = 50, the resultant zeolite product exhibited Si/Al = 49, determined by ICP-OES. The small amount of solvent used for the dry-gel synthesis limited the polymerization-depolymerization process of silicate anions allowing the Si/Al ratios to be maintained throughout the synthesis process. Overall, the MFI zeolite nanosponges obtained using the DGC route were comparable to the hydrothermally synthesized product.

4. Conclusion

The dry-gel synthesis of MFI zeolite nanosponges using a diquaternary ammonium surfactant ($C_{18\text{-}6\text{-}4}$) was realized in this work. The effect of various synthesis conditions, such as relative chamber humidity and basicity, on the final zeolite product was investigated to find the optimal gel composition for full crystallization of zeolite nanosponges. It was found that a relative humidity greater than 80% and a gel composition of 100 SiO_2/1 Al_2O_3/7.5 $C_{18\text{-}6\text{-}4}$/28.6 Na_2O/15 H_2SO_4/6000 H_2O allowed successful transformation of the zeolite precursor into crystalline zeolite nanosponges with full mesoporosity originating from the mesopore-generating function of the surfactant. In particular, when the humidity was controlled to be 80%, zeolite crystallization proceeded in a pseudomorphic manner resulting in the preservation of the initial dry gel morphologies in the final product. In excess water conditions of 100% humidity, the resultant zeolite nanosponge exhibited relatively large particle diameters compared with the result obtained at 80% humidity. An advantage of the dry-gel synthesis was that the autoclave volume was greatly reduced by filtration of the solvent water before heating at high pressure. With the benefit of reduced reactor volume, 100 g of MFI zeolite nanosponges were easily synthesized using a single autoclave with a volume of 1.5 L. The findings in this work would be helpful for the large-scale production of zeolite nanosponges.

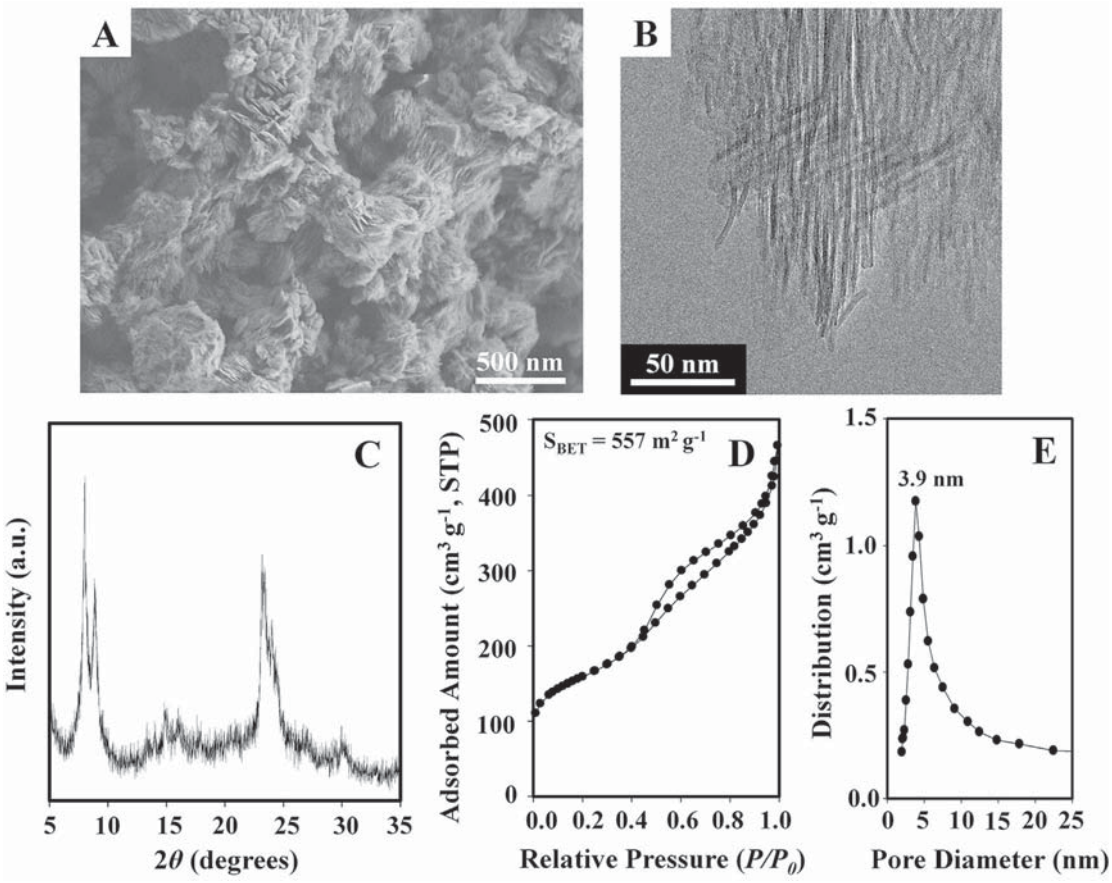

Fig. 4. Representative SEM image (A), TEM image (B), XRD pattern (C), N_2 adsorption-desorption isotherm (D), and BJH pore size distribution (E) of highly siliceous MFI zeolite nanosponges synthesized by DGC at 80% humidity.

Acknowledgements

This work was supported by IBS-R004-D1.

Appendix A. Supplementary data

Supplementary data related to this article can be found at http://dx.doi.org/10.1016/j.micromeso.2016.11.016.

References

[1] C.S. Cundy, P.A. Cox, Chem. Rev. 103 (2003) 663–702.
[2] C.S. Cundy, P.A. Cox, Micropor. Mesopor. Mater. 82 (2005) 1–78.
[3] K. Tanabe, W.F. Hölderich, Appl. Catal. A Gen. 181 (1999) 399–434.
[4] K. Varoon, X. Zhang, B. Elyassi, D.D. Brewer, M. Gettel, S. Kumar, J.A. Lee, S. Maheshwari, A. Mittal, C. Sung, M. Cococcioni, L.F. Francis, A.V. McCormick, K.A. Mkhoyan, M. Tsapatsis, Science 334 (2011) 72–75.
[5] M.A. Snyder, M. Tsapatsis, Angew. Chem. Int. Ed. 46 (2007) 7560–7573.
[6] W. Vermeiren, J.P. Gilson, Top. Catal. 52 (2009) 1131–1161.
[7] J. Pérez-Ramíez, C.H. Christensen, K. Egeblad, C.H. Christensen, J.C. Groen, Chem. Soc. Rev. 37 (2008) 2530–2542.
[8] K. Na, G. Somorjai, Catal. Lett. 145 (2015) 193–213.
[9] X. Meng, F. Nawaz, F. Xiao, Nano Today 4 (2009) 292–301.
[10] R. Chal, C. Géradin, M. Bulut, S. van Donk, ChemCatChem. 3 (2011) 67–81.
[11] I.I. Ivanova, A.S. Kuznetsov, V.V. Yuschenko, E.E. Knyazeva, Pure Appl. Chem. 76 (2004) 1647–1657.
[12] R.A. Beyerlein, C. Choi-Feng, J.B. Hall, B.J. Huggins, G.J. Ray, Top. Catal. 4 (1997) 27–42.
[13] B.A. Williams, S.M. Babitz, J.T. Miller, R.Q. Snurr, H.H. Kung, Appl. Catal. A Gen 177 (1999) 161–175.
[14] J.C. Groen, W. Zhu, S. Brouwer, S.J. Huynink, F. Kapteijn, J.A. Moulijn, J. Pérez-Ramíez, J. Am. Chem. Soc. 129 (2007) 355–360.
[15] P. Eliášová, M. Opanasenko, P.S. Wheatley, M. Shamzhy, M. Mazur, P. Nachtigall, W.J. Roth, R.E. Morris, J. Čejka, Chem. Soc. Rev. 44 (2015) 7177–7206.
[16] L. Tosheva, V.P. Valtchev, Chem. Mater. 17 (2005) 2494–2513.
[17] H. Wang, T.J. Pinnavaia, Angew. Chem. Int. Ed. 45 (2006) 7603–7606.
[18] C. Madsen, C.J.H. Jacobsen, Chem. Commun. (1999) 673–674.
[19] J. Koo, N. Jiang, S. Saravanamurugan, M. Bejblová, Z. Musilová, J. Čejka, S. Park, J. Catal. 276 (2010) 327–334.
[20] K. Na, C. Jo, J. Kim, K. Cho, J. Jung, Y. Seo, R.J. Messinger, B.F. Chmelka, R. Ryoo, Science 333 (2011) 328–332.
[21] J. Zhou, Z. Hua, Z. Liu, W. Wu, Y. Zhu, J. Shi, ACS Catal. 4 (2011) 287–291.
[22] M. Choi, K. Na, J. Kim, Y. Sakamoto, O. Terasaki, R. Ryoo, Nature 461 (2009) 246–249.
[23] W. Park, D. Yu, K. Na, K.E. Jelfs, B. Slater, Y. Sakamoto, R. Ryoo, Chem. Mater. 23 (2011) 5131–5137.
[24] J. Jung, C. Jo, K. Cho, R. Ryoo, J. Mater. Chem. 22 (2012) 4637–4640.
[25] K. Na, M. Choi, W. Park, Y. Sakamoto, O. Terasaki, R. Ryoo, J. Am. Chem. Soc. 132 (2010) 4169–4177.
[26] C. Jo, K. Cho, J. Kim, R. Ryoo, Chem. Commun. 50 (2014) 4175–4177.
[27] J. Kim, K. Cho, S. Lee, R. Ryoo, Catal. Today 243 (2015) 103–108.
[28] J. Kim, R. Ryoo, M.V. Opanasenko, M.V. Shamzhy, J. Čejka, ACS Catal. 4 (2015) 2596–2604.
[29] J. Kim, S. Lee, K. Cho, K. Na, C. Lee, R. Ryoo, ACS Catal. 4 (2014) 3919–3927.
[30] X. Meng, F. Xiao, Chem. Rev. 114 (2014) 1521–1543.
[31] M. Matsukata, M. Ogura, T. Osaki, P.R.H.P. Rao, M. Nomura, E. Kikuchi, Top. Catal. 9 (1999) 77–92.
[32] S.P. Naik, A.S.T. Chiang, R.W. Thompson, J. Phys. Chem. B 107 (2003) 7006–7014.
[33] W. Xu, J. Dong, J. Li, J. Li, F. Wu, J. Chem. Soc. Chem. Commun. (1990) 755–756.
[34] L. Ren, Q. Wu, C. Yang, L. Zhu, C. Li, P. Zhang, H. Zhang, X. Meng, F. Xiao, J. Am. Chem. Soc. 134 (2012) 15173–15176.
[35] Y. Jim, Q. Sun, G. Qi, C. Yang, J. Xu, F. Chen, X. Meng, F. Deng, F. Xiao, Angew. Chem. Int. Edit. 52 (2013) 9172–9175.
[36] Y. Qiu, L. Wang, X. Zhang, G. Liu, RSC Adv. 5 (2015) 78238–78246.
[37] B. Chen, Y. Huang, Micropor. Mesopor. Mater. 143 (2011) 14–21.
[38] X. Cheng, J. Mao, X. Lv, T. Hua, X. Cheng, Y. Long, Y. Tang, J. Mater. Chem. A 2 (2014) 1247–1251.
[39] R. Cai, Y. Liu, S. Gu, Y. Yan, J. Am. Chem. Soc. 132 (2010) 12776–12777.
[40] M. Matsukata, N. Nishiyama, K. Ueyama, Microporous Mater. 1 (1993) 219–222.
[41] C. Chang, H.J. Cho, Z. Wang, X. Wang, W. Fan, Green Chem. 17 (2015) 2943–2951.
[42] D. Hu, Q.H. Xia, X.H. Lu, X.B. Luo, Z.M. Liu, Mater. Res. Bull. 43 (2008) 3553–3561.
[43] H.S. Cho, R. Ryoo, Micropor. Mesopor. Mater. 151 (2012) 107–112.
[44] C. Song, H. Yang, Y. Wang, Y. Feng, X. Shi, H. Duan, Asia Pac. J. Chem. Eng. in press, doi:10.1002/apj.2018.